Near-Field Shaped Transmitarray Antennas: Synthesis and Impact of Phase Quantization

Sergio M. Feito[1,2], Francesco Foglia Manzillo[2], Antonio Clemente[2], Manuel Arrebola[1]
[1] Group of Signal Theory and Communications, Universidad de Oviedo, Gijón, Spain, {UO191808, arrebola}@uniovi.es
[2] CEA - Leti, Univ. Grenoble-Alpes, F-38000 Grenoble, France, {francesco.fogliamanzillo, antonio.clemente}@cea.fr

***Abstract*—In this work, a procedure based on the Intersection Approach, is proposed to synthesize the near-field pattern of transmitarray antennas. First, the model for the computation of the amplitude and phase of the electric field in the near-field region is described and validated by comparison with full-wave simulations. Next, the proposed phase-only synthesis algorithm is detailed. Using fast Fourier transforms, it iteratively seeks for a feasible aperture phase profile that can fit near-field pattern constraints. The procedure is applied to synthesize a transmitarray generating a near-field shaped pattern on a plane parallel to the aperture. The impact of a uniform phase quantization on the near-field pattern and amplitude is analysed to provide design guidelines.**

***Index Terms*—Near-field synthesis, Intersection Approach, Fourier analysis, transmitarray antenna.**

I. INTRODUCTION

The analysis and synthesis of near-field antennas have triggered an increasing interest for multiple emerging applications, such as wireless power transfer [1], hyperthermia and medical scanners [2], or next-generation smart access points [3]. For these applications, the radiated near-field (NF) must be shaped either in specific planes, or in a volume [4].

Spatially fed arrays (SFA), such as transmitarray (TA), metalens and reflectarray (RA) antennas, represent an effective and energy-efficient solution to shape and control the near-field distribution in the Fresnel region. TAs comprise radiating elements (unit cells), which re-radiate an incident electromagnetic field after locally introducing a phase shift on it. By properly designing the unit cells (UCs) and their distribution on the TA aperture, the radiated electromagnetic field can be tailored with negligible losses, as opposed to phased array architectures.

Several procedures for the synthesis of SFAs have been proposed in the literature. They are based on different mathematical methods, such as the Intersection Approach (IA) [5] or convex optimization [6]. However, most works deal with far-field synthesis, while only a few procedures for near-field shaping have been presented [7]-[9].

The work in [9] focuses on the synthesis of non-diffractive beams. In the TA synthesis procedure presented in [8], the NF is calculated as the sum of the far-field (FF) contributions of each cell and not using a single Fourier transform of the aperture field, increasing the computation time. Moreover, most NF-shaped TAs presented in the literature are actually 2.5-D dielectric discrete lenses [8], [9], where the height of each UC is tuned to approximate the optimal phase shift distribution. This approach is not useful for the design of high-efficiency TAs realized in planar technologies, where only a discrete set of phase shifts is usually selected to enhance the bandwidth and reduce the complexity of the manufacturing process.

In this work, we generalize the use of the Intersection Approach to the synthesis of planar and electronically reconfigurable TAs, which generally enable coarse phase quantization [10], [11]. To this end, we propose a fast tool for arbitrarily shaping the NF pattern, on a plane parallel to the aperture. In addition, the impact of an *N*-bit phase quantization on the optimized phase profile is investigated. Numerical results are presented to validate the analysis model and demonstrate the effectiveness of the synthesis procedure.

II. TRANSMITARRAY DEFINITION AND ANALYSIS

A. Transmitarray model

The structure of the TA under analysis is illustrated in Fig. 1. The antenna comprises a focal source and a planar array of $M \times N$ UCs, of the same size, located at a distance F from the feed. The dimensions of the edges of the lens are D_x and D_y, while the distances between the centers of adjacent UCs are d_x and d_y along x- and y-axis, respectively.

The source illuminates the array, and its UCs locally modify the impinging field on its receiving side, transforming it into the field $\vec{E}_{AP}$ on the radiating aperture (transmitting side). The UCs are generally designed to introduce minimum losses. Therefore, they mainly introduce a phase shift on the incident field and/or a polarization manipulation. The distribution of the UCs, and thus the phase of $\vec{E}_{AP}$ must be optimized to obtain a desired near-field pattern.

Assuming that the field distribution is uniform within each UC, the electric tangential field $\vec{E}_{AP}$ over the transmitting layer of the TA can be written as

$$\vec{E}_{AP}(x_m, y_n) = \boldsymbol{T}^{mn} \cdot \vec{E}_{inc}(x_m, y_n), \qquad (1)$$

where $\vec{E}_{inc}^{mn}(x_m, y_n)$ is the incident field received from the feed, x_m and y_n are the coordinates of the center of the *mn-th* cell. The transmission coefficient matrix $\boldsymbol{T}^{mn}$ characterizes the transmission properties of the *mn-th* cell.

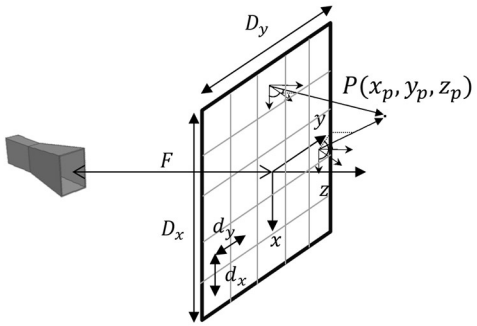

Fig. 1. Sketch of the transmitarray geometry.

Once the tangential field on the transmitting side is obtained, the field radiated by the TA is calculated using its plane-wave expansion, leveraging on the fast Fourier transform (FFT) [4]. Neglecting the direct radiation from the feed, the *i*-component E_{NF}^{i} of the near-field emitted in free space, on a plane $z = z_0$, parallel to the radiating aperture, can be computed as:

$$E_{NF}^{i}(x, y, z_0) = \frac{1}{4\pi^2}\mathcal{F}^{-1}\{g_p \mathcal{F}\{E_{AP}(x, y)\}\}, \quad (2)$$

where $\mathcal{F}$ and $\mathcal{F}^{-1}$ indicate the direct and inverse Fourier transform operators, respectively. Furthermore, we assume that the aperture field has a single non-null component E_{AP}. The factor $g_p = e^{-jk_z z_0}$ [12] is equivalent to a translation in space by z_0 along the *z*-axis, and the *z*-component k_z of the wave vector is defined as

$$k_z = \begin{cases} \sqrt{k^2 - k_x^2 - k_y^2}, k^2 \geq k_x^2 + k_y^2 \\ -j\sqrt{-k^2 + k_x^2 + k_y^2}, k^2 \leq k_x^2 + k_y^2 \end{cases}, \quad (3)$$

being k the free-space propagation constant, k_x and k_y the spatial frequencies extending over the entire spectrum ($-\infty < k_x, k_y < \infty$).

B. Model validation

In order to validate the model described in Section II-A, a near-field focusing TA has been designed, using the set of 16 UCs presented in [13]. A comparison of the numerical predictions of the model with the results obtained through the full-wave simulation of the TA is presented next.

A NF-focusing TA comprising 24×24 square UCs, with d_x=d_y =0.35λ, where λ is the free-space wavelength at the operating frequency of 140 GHz, is considered. It is fed by a 10-dBi pyramidal horn aligned with the centre of the array, at a distance $F = 0.8D_x$. The phase profile of the TA is derived using the conjugate phase approach [3] to focus the field in the point $P = (0, 0, 0.1D_{ff})$, where $D_{ff} \cong 141\lambda$ is the far-field distance at 140 GHz. In particular, the phase shift introduced by the *mn*-th UC, at a distance r_{mn} from *P* is set to:

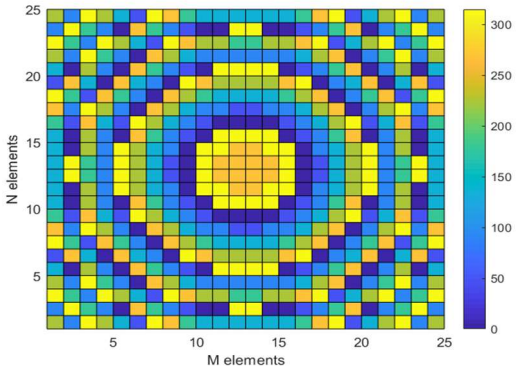

Fig. 2. Spatial profile of the UC phase shifts (in degrees) of the 24×24 TA designed using phase-conjugate approach to focus the *y*-component of the electric field in *P* (0,0, 14.1λ).

$$\chi_{mn} = \frac{2\pi}{\lambda} r_{mn} - \angle E_{inc,mn} \quad (4)$$

This technique enables the maximization of the near-field amplitude is in *P*, except for a shift due to the field spreading factor [14]. However, it does not allow one to control the shape of the near-field pattern.

Fig. 2 shows the obtained 4-bit quantized TA phase profile. The phases of the UC transmission coefficients, simulated under normal incident in a periodic environment, are almost uniformly spaced in the 2π range. These UCs comprise two wire grid polarizers on the outer layers so that they rotate by 90º the polarization of the incident field. Thus, the *x*-polarized field radiated by the horn is converted into an almost purely *y*-polarized aperture field. Therefore, the effect of the spillover on the *y*-component of the electric field is negligible. The incident field on the array is found using the simulated far-field radiation pattern of the horn. Moreover, the complex transmission coefficients t_{yx} of the 16 UCs were considered in the computation of the near-field.

The *x*-cut of the near-field pattern (*y*-component) on the focusing plane $z = 14.1\lambda$ is shown in Fig. 3. The field predicted by the proposed model is in tight agreement with that obtained from the full-wave simulation of the TA.

It is worth to observe that the model accurately predicts the amplitude and not only the normalized pattern of the near-field. The difference between the computed and simulated peak value is only 0.7 dB. Most of the state-of-art works on near-field focusing and shaping TAs [7], [9] only compare normalized patterns.

III. Synthesis Procedure using Intersection Approach

The method used for the synthesis is based on the Intersection Approach [15]. In this work, two masks (T_{upper} and T_{lower}) are enforced as lower and upper bounds for the near-field amplitude.

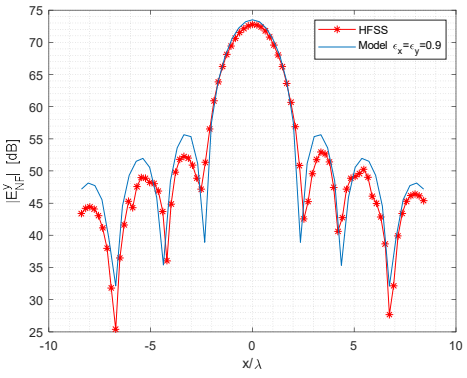

(a)

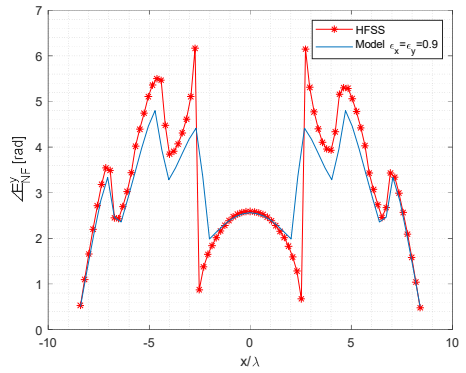

(b)

Fig. 3. Full-wave simulation comparison with the model. (a) Comparison of the y-component of the radiated field at $z = 0.1$ times the far-field distance. (b) Comparison of the phase of the y-component of the radiated field at $z = 0.1$ times the far-field distance.

The algorithm iteratively applies two operators: the forward propagator ($\mathcal{P}$) described in (3) and the backward propagator ($\mathcal{B}$) described as:

$$E_{AP}(x,y) = \frac{1}{4\pi^2}\mathcal{F}^{-1}\left\{g_b\mathcal{F}\left\{E^i_{NF}(x,y,z_0)\right\}\right\}, \qquad (5)$$

where $g_b = e^{+jk_z h}$ and k_z is defined as (3), with the exception that when the second condition ($k^2 \leq k_x^2 + k_y^2$) is true, the expression becomes positive.

Following the chart in Fig. 4, starting from a given tangential field distribution over the aperture, the NF is calculated through the forward propagator ($\mathcal{P}$), considering each UC of the TA as a rectangular aperture antenna with uniform field distribution [16]. This operation outputs a near-field (E^i_{NF}) which, generally, does not satisfy the constraints enforced. Therefore, a modified near-field $\tilde{E}_{NF}$, fulfilling the radiation mask, is built. While its phase is left unmodified, its amplitude is set as:

$$|\tilde{E}^{i}_{NF}| = \begin{cases} T_{upper}\,; & if\ \ E_{NF} \geq T_{upper} \\ T_{lower}\,; & if\ \ E_{NF} \leq T_{lower} \\ |E^i_{NF}|; & otherwise \end{cases} \qquad (6)$$

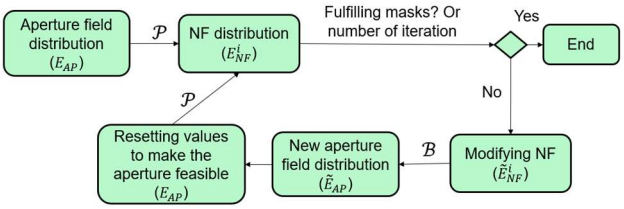

Fig. 4. Flowchart of the classical Intersection Approach used for the synthesis of near-field shaping TAs.

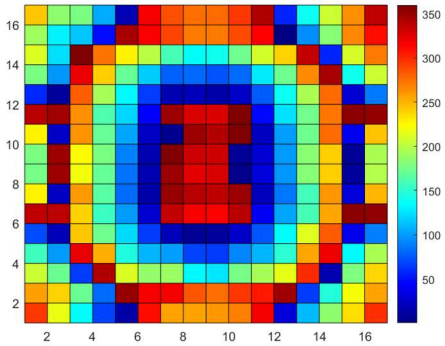

Fig. 5. Synthesised phase distribution in degrees introduced by the unit cells of the 16×16 near-field shaped TA.

At this point, using the backward propagation ($\mathcal{B}$), the field distribution $\tilde{E}_{AP}$ generating $\tilde{E}^i_{NF}$ is found. Since the amplitude of the field on the TA aperture depends on the incident field, it is not guaranteed that $\tilde{E}^i_{ap}$ can be a feasible tangential field. In practice, only its phase can be tailored by properly distributing the UCs in the TA. Therefore, the following field distribution over the aperture (E_{AP}) is specified after the backward propagation and used for the next iteration of the algorithm:

$$E_{AP} = \begin{cases} |E_{inc}|e^{j\angle\tilde{E}_{ap}}\,; & |x| \leq \frac{D_x}{2}\,, |y| \leq \frac{D_y}{2} \\ 0\,; & otherwise \end{cases} \qquad (7)$$

By iteratively performing this procedure, a solution that satisfies both physical restrictions on the aperture field and the NF pattern constraints may be found.

A. Numerical results: a shaped-beam near-field pattern

An example of TA synthesis for near-field shaping is discussed. The objective is to generate a fan-beam near-field pattern, on a plane at a distance $z = 14.8\lambda$, with a -3-dB spot of $2\lambda \times 7.5\lambda$. A maximum 1.5-dB amplitude ripple is required in the flat-top region of the y-cut. For achieving this near-field pattern, a 16×16 TA fed by a 10-dBi horn was considered. The UC size is λ/2×λ/2, being λ the wavelength at the optimization frequency. The feed is at a distance from the lens $F = 0.8\ D$, where $D = 8\ \lambda$ is the length of the edge of the lens. Its simulated far-field pattern was used to calculate the incident field on the TA.

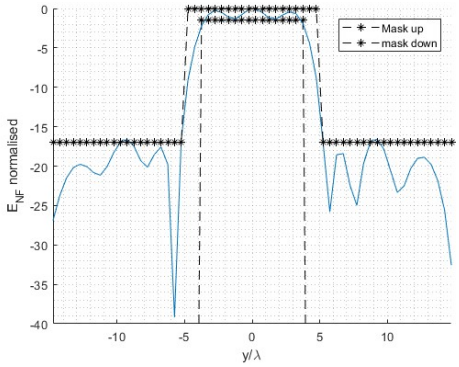

Fig. 6. NF pattern (x=0 cut) of the synthesized 16×16 TA, at a distance of 14.8λ from the TA radiating aperture, using the UC phase profile of Fig. 5.

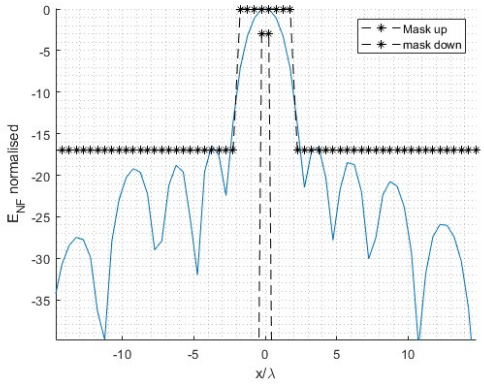

Fig. 7. NF pattern (y=0 cut) of the synthesized 16×16 TA, at a distance of 14.8λ from the TA radiating aperture, using the UC phase profile of Fig. 5.

The aperture-field distribution compensating the phase of the incident field and realizing a broadside far-field pencil beam was used as the seed of the algorithm. Despite the initial near-field pattern is very different from the desired one, the proposed synthesis procedure is able to converge fulfilling the enforced masks. The procedure achieves this in 260 s, after iterating about 900 times. The synthesized phase profile, introduced by the lens on the incident field, is represented in Fig. 5. Even if no symmetry constraints were prescribed, it is quite symmetric with respect to the centre of the aperture, as one would physically expect for generating this pattern.

The y- and x-cut of the near-field pattern on the target plane are shown, along with the enforced mask, in Fig. 6 and Fig. 7, respectively.

B. *Impact of phase quantization*

In Section III-A, we assumed that the UCs could introduce any phase shift value, and thus perfectly realize the optimal phase profile. In practical designs, especially for electronically reconfigurable TAs, only a few different UCs are used, providing a discrete set of phase shifts. The design of a large number of UCs would indeed be time-consuming, technologically challenging and narrow the common operating bandwidth. Thus, it is key to evaluate, after the synthesis, the impact of the phase quantization on the near-field. The results will generally depend on the mask and the

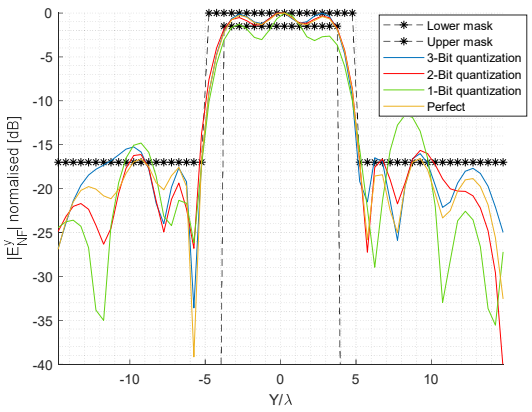

Fig. 8. NF pattern (x=0 cut) of the 16×16 synthesized TA, at a distance of 14.8λ from the aperture, for different n-bit quantization of the optimal phase distribution of Fig. 5.

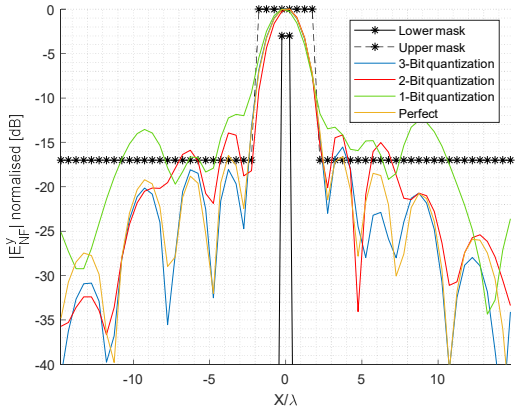

Fig. 9. NF pattern (y=0 cut) of the 16×16 TA, at a distance of 14.8λ from the aperture, for different n-bit quantization of the optimal phase distribution of Fig. 5.

plane where it is enforced. However, the synthesized TA discussed in Section III-A represents a relevant example, as its phase profile is relatively fast-varying, due to the challenging mask constraints. Thus, the synthesized phase profile was approximated using three sets of 2^n UCs, with n =1, 2, 3. The phases of the transmission coefficients of each set are uniformly distributed in the [0, 2π) range (uniform n-bit quantization).

Figure 8 and Fig. 9 show the NF patterns obtained for different n. It can be observed that the x-cut is more sensitive to a coarse phase quantization. On the other hand, the y-cut seems more robust. However, the 1-bit quantization significantly increases the ripple in the flat-top region.

Figure 10 shows the amplitude of the y-component of the electric field radiated by the TA as a function of distance from the aperture, along the z-axis. This distance is normalized to the far-field distance. As expected, the peak amplitude decreases with the phase resolution, due to the increase of the phase error. The amplitude loss at z = 14.8λ is 2.7 dB, 0.6 dB and 0.25 dB for a 1-bit, 2-bit and 3-bit phase quantization, respectively.

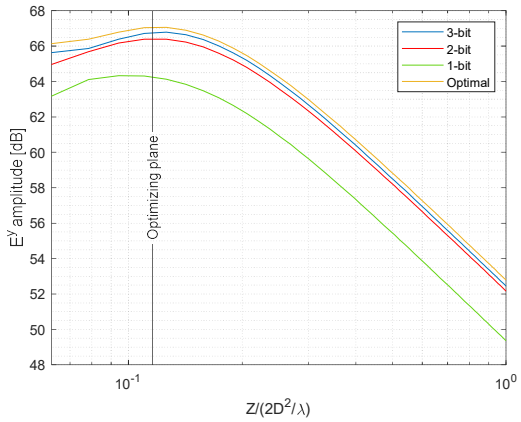

Fig. 10. Amplitude of the *y*-component of the electric field radiated by the synthesised 16×16 TA, as a function of the distance from the aperture. Results obtained for different *n*-bit quantization of the optimal phase distribution of Fig. 5 are presented.

The analysis of the near-field pattern distortion and of the amplitude loss due to phase quantization shows that a 3-bit quantization or finer of the optimal phase can fulfil the masks in most of the points where they are defined.

IV. Conclusion

In this work, a model for the analysis and synthesis of the near field radiated by a transmitarray antennas has been proposed and validated via full-wave simulation. As opposed to most works in the literature, the model accurately predicts not only the normalized near-field pattern, but also the amplitude of the electric field. Based on this model, a phase-only synthesis procedure that allows to arbitrarily shape a component of the electric field on planes parallel to the aperture is proposed. The algorithm leverages on the Intersection Approach and is computationally efficient. A 16×16 transmitarray generating a fan-beam near-field pattern has been synthesized in a few seconds.

The degradation of the near-field pattern and the amplitude loss due to a uniform quantization of the optimal phase profile have been assessed. A phase quantization finer than a 3-bit one is necessary to approximate the optimal results, a good performance. Nevertheless, a relatively good performance is achieved for 2-bit quantization. This result could pave the way for the use of relatively simple electronically reconfigurable transmitarrays for dynamic near-field shaping.

Acknowledgment

This work was supported in part by MICIN/AEI/10.13039/501100011033 within the project PID2020-114172RB-C21; and by the Gobierno del Principado de Asturias under project AYUD/2021/51706.

References

[1] A. Razavi, R. Maaskant, J. Yang, and M. Viberg, “Optimal aperture Distribution for near-field detection of foreign objects in lossy media,” in *Proc. IEEE-APS Topical Conf. Antennas Propag. Wireless Comm.*, Palm Beach, Aruba, 2014, pp. 659–662.

[2] X. He, W. Geyi, and S. Wang, “Optimal design of focused arrays for microwave-induced hyperthermia,” *IET Microw., Antennas Propag.*, vol. 9, no. 14, pp. 1605–1611, 2015.

[3] A. Buffi, A. A. Serra, P. Nepa, H. T. Chou, and G. Manara, “A focused planar microstrip array for 2.4 GHz RFID readers,” *IEEE Trans. Antennas Propag.*, vol. 58, no. 5, pp. 1536–1544, Mar. 2010.

[4] I. Iliopoulos, M. Casaletti, R. Sauleau, P. Pouliguen, P. Potier and M. Ettorre, "3-D Shaping of a Focused Aperture in the Near Field," *IEEE Trans. Antennas Propag.*, vol. 64, no. 12, pp. 5262-5271, Dec. 2016.

[5] D. R. Prado, J. A. López Fernández, M. Arrebola, M. R. Pino and G. Goussetis, "General Framework for the Efficient Optimization of Reflectarray Antennas for Contoured Beam Space Applications," *IEEE Access*, vol. 6, pp. 72295-72310, 2018.

[6] F. Foglia Manzillo, O. Koutsos, B. Fuchs, R. Sauleau and A. Clemente, "Synthesis and Characterization of a Focused-Beam Transmitarray Antenna at 300 GHz," *Eur. Conf. Antennas and Propag. (EuCAP)*, 2022.

[7] Á. F. Vaquero. M. Arrebola and M. R. Pino, “Development of techniques for the analysis and synthesis of spatially-fed arrays for emerging applications in near-field”, *PhD thesis*, Sept., 2021.

[8] S. Loredo, G. León and E. G. Plaza, "A Fast Approach to Near-Field Synthesis of Transmitarrays," *IEEE Antennas Wirel. Propag. Lett.*, vol. 20, no. 5, pp. 648-652, May 2021.

[9] G. -B. Wu, K. F. Chan and C. H. Chan, "3-D Printed Terahertz Lens to Generate Higher Order Bessel Beams Carrying OAM," *IEEE Trans. Antennas Propag.,* vol. 69, no. 6, pp. 3399-3408, June 2021.

[10] A. Clemente, F. Foglia Manzillo, M. Śmierzchalski and R. Sauleau, "Electronically-Steerable Transmitarray Antennas for SATCOM Terminals: a System Perspective," *Int. Workshop Antenna Tech. (iWAT)*, 2020, pp. 1-4.

[11] F. Foglia Manzillo, M. Smierzchalski, J. Reverdy and A. Clemente, "A Ka-band Beam-Steering Transmitarray Achieving Dual-Circular Polarization," *15th Eur. Conf. Antennas Propag. (EuCAP),* 2021.

[12] M. Ettorre et al., "On the Near-Field Shaping and Focusing Capability of a Radial Line Slot Array," *IEEE Trans. Antennas Propag*., vol. 62, no. 4, pp. 1991-1999, April 2014.

[13] F. Foglia Manzillo, A. Hamani, A. Siligaris, A. Clemente and J. L. González-Jiménez, "A highly directive D-Band antenna module comprising a flat discrete lens and an active feed," Proc. *IEEE Int. Symp. Antennas Propag. (AP-S/URSI)*, pp. 321-322, Denver, USA, July 2022.

[14] R. Hansen, "Focal region characteristics of focused array antennas," *IEEE Trans. Antennas Propag*., vol. 33, no. 12, pp. 1328-1337, December 1985.

[15] J. A. Zornoza and J. A. Encinar, “Efficient phase-only synthesis of contouredbeam patterns for very large reflectarrays,” *Int. J. RF Microw. Comput. Eng*., vol. 14, no. 5, pp. 415–423, Sep. 2004.

[16] C. A. Balanis, Antenna Theory: Analysis and Design, 3rd Ed. Hoboken, NJ, USA: Wiley Interscience, 2005.